Convection in future winter storms over Northern Europe

Berthou, S. ORCID: https://orcid.org/0000-0002-9164-0841, J Roberts, M. ORCID: https://orcid.org/0000-0001-6128-6979, Vannière, B. ORCID: https://orcid.org/0000-0001-8600-400X, Ban, N. ORCID: https://orcid.org/0000-0002-1672-3655, Belušić, D. ORCID: https://orcid.org/0000-0002-5665-3866, Caillaud, C. ORCID: https://orcid.org/0000-0003-2317-4129, Crocker, T. ORCID: https://orcid.org/0000-0001-7761-5546, de Vries, H. ORCID: https://orcid.org/0000-0002-6124-1102, Dobler, A., Harris, D. ORCID: https://orcid.org/0000-0003-4369-4674, J Kendon, E. ORCID: https://orcid.org/0000-0003-1538-2147, Landgren, O. ORCID: https://orcid.org/0000-0002-6264-8502 and Manning, C. ORCID: https://orcid.org/0000-0001-5364-3569 (2022) Convection in future winter storms over Northern Europe. Environmental Research Letters, 17 (11). 114055. ISSN 1748-9326 doi: 10.1088/1748-9326/aca03a Available at https://centaur.reading.ac.uk/109475/

ENVIRONMENTAL RESEARCH
LETTERS

LETTER • OPEN ACCESS

Convection in future winter storms over Northern Europe

IOP Publishing Environ. Res. Lett. 17 (2022) 114055 https://doi.org/10.1088/1748-9326/aca03a

ENVIRONMENTAL RESEARCH
LETTERS

OPEN ACCESS

RECEIVED
22 July 2022

REVISED
1 November 2022

ACCEPTED FOR PUBLICATION
4 November 2022

PUBLISHED
16 November 2022

LETTER

Convection in future winter storms over Northern Europe

Ségolène Berthou[1,*], Malcolm J Roberts[2], Benoît Vannière[3], Nikolina Ban[4,5], Danijel Belušić[6,7], Cécile Caillaud[8], Thomas Crocker[1], Hylke de Vries[9], Andreas Dobler[10], Dan Harris[1], Elizabeth J Kendon[2,11], Oskar Landgren[10] and Colin Manning[12]

[1] Met Office, Exeter, United Kingdom
[2] Met Office Hadley Centre, Exeter, United Kingdom
[3] National Centre for Atmospheric Science, Reading, United Kingdom
[4] Institute for Atmospheric and Climate Science, ETH Zürich, Zürich, Switzerland
[5] Department of Atmospheric and Cryospheric Sciences, University of Innsbruck, Innsbruck, Austria
[6] Swedish Meteorological and Hydrological Institute (SMHI), Norrköping, Sweden
[7] University of Zagreb, Zagreb, Croatia
[8] CNRM, Université de Toulouse, Météo-France, CNRS, Toulouse, France
[9] Royal Netherlands Meteorological Institute (KNMI), De Bilt, The Netherlands
[10] Norwegian Meteorological Institute (MET Norway), Oslo, Norway
[11] University of Bristol, Bristol, United Kingdom
[12] School of Civil Engineering and Geosciences, University of Newcastle, Newcastle-upon-Tyne, United Kingdom
[*] Author to whom any correspondence should be addressed.

E-mail: segolene.berthou@metoffice.gov.uk

Keywords: convection-permitting models, precipitation, winter storms, extratropical cyclones, climate change, convection

Supplementary material for this article is available online

Abstract

Precipitation within extratropical cyclones is very likely to increase towards the end of the century in a business-as-usual scenario. We investigate hourly precipitation changes in end-of-century winter storms with the first km-scale model ensemble covering northwest Europe and the Baltic region. This is an ensemble that explicitly represents convection (convection permitting models (CPMs)). Models agree that future winter storms will bring 10%–50% more precipitation, with the same level of light precipitation but more moderate and heavy precipitation, together with less frequent frozen precipitation. The warm sector precipitation rates will get closer (up to similar) to those in present-day autumn storms, along with higher convective available potential energy and convective inhibition, suggesting more convection embedded in storms. To the first order, mean hourly precipitation changes in winter storms are driven by temperature increase (with little relative humidity changes) and storm dynamical intensity (more uncertain), both captured by regional climate models (RCMs). The CPMs agree with this, and in addition, most CPMs show more increase in intense precipitation in the warm sector of storms compared to their parent RCM.

1. Introduction

Climate change is likely to bring milder and wetter winters to Northern Europe (Doblas-Reyes *et al* 2021). Given the current vulnerability of northern European societies to extensive winter flooding (Muchan *et al* 2015), we need to better understand how the nature of winter precipitation will change. Precipitation is expected to intensify in a warming climate, in the first order due to increased water holding capacity of the atmosphere (Fischer and Knutti 2016). In regions and seasons not limited in atmospheric moisture supply, this will translate into an increase in mean precipitation, like in Northern Europe in winter (Poujol *et al* 2021). Global climate models project more precipitation per storm (Hawcroft *et al* 2018, Catto *et al* 2019) but dynamical changes in storm tracks, storm numbers and storm intensity are less certain (Zappa *et al* 2013, Fereday *et al* 2018, Catto *et al* 2019). The most robust dynamical changes over Europe in winter are an eastward extension of North Atlantic jet stream, which means an increase in storm numbers over the UK and Baltic regions (Harvey *et al* 2020, Albern *et al* 2021) and an increase in dynamically extreme storms (Priestley and Catto 2021).

With the growing availability of ensembles of km-scale models at climate scales (Ban *et al* 2021, Pichelli *et al* 2021), we can examine finer-scale hourly

precipitation processes in future winter (FW) storms. Indeed, case studies show that many precipitation processes in mid-latitude cyclones are improved at km-scale modelling: shallow convection in the cold sector/dry intrusion overlaying a warmer surface (Grossman and Betts 1990), slantwise convection releasing conditional symmetric instability associated within fronts (Lean and Clark 2003, Glinton *et al* 2017, Chen *et al* 2021), better representation of frontal structures, dry intrusion overrunning the warm sector (Browning 1997), embedded convection in warm conveyor belt and cold fronts (Neiman *et al* 1993, Rasp *et al* 2016, Oertel *et al* 2019).

In this study, we investigate how the nature of hourly precipitation and its rate may change in FW storms in a business-as-usual RCP8.5 end-of-century scenario. A change in the nature of precipitation within storms will have strong local impacts through its modulation of surface runoff and will also affect storm predictability through modification of the upper-level potential vorticity field by convection (Oertel *et al* 2020).

After showing that the sub-sampling of models that we use is representative of the uncertainty range of a larger ensemble, we show how precipitation rates change in different sectors of the storms. We then investigate reasons behind the diversity of storm precipitation projections between models and finally examine changes in convective properties in the model with the highest level of warming.

2. Data and methods

2.1. Data

We use five pairs of convection permitting models (CPMs) at 2–3 km resolution, double nested in 12 km regional climate models (convection-parameterised) (RCMs) and general circulation models (GCMs) (table 1). The model evaluation papers are listed in table 1. CPMs were shown to better represent hourly precipitation characteristics. KNMI and HCLIMcom use the same CPM (but different RCM and GCM), while CNRM also uses a similar CPM. ETHZ uses a pseudo-global warming (PGW) approach: the present-day RCM is driven by ERA-interim reanalysis and the future RCM by ERA-interim plus a 3D Max Planck Institut-Earth System Model-Low Resolution (MPI-ESM-LR)-derived thermodynamical climate change signal which includes slow circulation changes (Brogli *et al* 2019, Hentgen *et al* 2019). By design, the number of extratropical cyclones entering the domain is the same between the present and future ETHZ runs. MOHC does not use an intermediate nest since it is driven by a 25 km GCM. We use the 25 km GCM as reference (and call it RCM for simplicity in the figures). KNMI downscales different members of their GCM ensemble for the present-day and future time slices to be able to get a reasonably unbiased response with respect to the ensemble mean response in a number of parameters (De Vries, personal communication).

We compare a ten-year historic time-period with a ten-year end-of-century time period. ETHZ and MOHC simulations do not share the exact same dates as they were run before a common protocol was agreed in the European Climate Prediction project (EUCP). Both the GCM and time period difference mean that ETHZ has the smallest warming signal and MOHC the strongest (see section 3.1). The future scenario is RCP8.5.

Figure 1 shows the diversity of CPM domains covering Northern Europe. The reason for this choice was to keep the computing costs reasonable while covering most of Europe within the EUCP project. CPM data is regridded to the RCM grid for a fair comparison, except in section 3.4, where the CPM is analysed on its native grid.

2.2. Methods

2.2.1. Tracking algorithm

We track the storms using a widely used feature tracking package called TempestExtremes (Zarzycki and Ullrich 2017, Ullrich *et al* 2021). Candidates are identified as local minima in the sea level pressure (SLP). Candidates with SLP increasing by 150 Pa over a 5° radius around them are selected (closed contour criteria). Individual candidates are then stitched together into tracks based on further criteria (e.g. minimum lifetime, maximum distance between each point, minimum total distance). The same parameters were used for all RCMs (supplementary material).

2.2.2. Selection of tracks

Tracks are selected within subregions centred on the CPM domain (boxes in figure 1). The regions are slightly different between CPMs, but always remain within the region of mean precipitation increase in all CPMs. We show that the processes at play are consistent between models and regions. Sensitivity tests to the exact region definition showed little impact on the results (not shown). The driving model is masked to match the CPM domain for a fair comparison.

Once the track is identified in the RCM, we find the associated minimum SLP in the CPM within a 3° radius, commonly used in inter-tracking comparisons (Neu *et al* 2013). For all models, the CPM SLP minima stays within 2° of the RCM one for at least 75% of the storm frames. The CNRM CPM is closest to its parent RCM and MOHC CPM is furthest away, potentially because of the large domain and GCM/CPM configuration differences (Berthou *et al* 2020).

2.2.3. Storm size and within-storm variables

Once the storm is selected, SLP, precipitation and wet bulb potential temperature (WBPT) are used within a 10° radius of the SLP minima, which is large enough to encompass some of the trailing front and

Table 1. List of simulations. Acronym definition: HARMONIE-Climate community (HCLIMcom), Swedish Meteorological and Hydrological Institute (SMHI), Finnish Meteorological Institute (FMI), Danish Meteorological Institute (DMI), Norwegian Meteorological Institute (Met Norway), National Centre of Meteorological Research (CNRM), Royal Netherlands Meteorological Institute (KNMI), Swiss Federal Institute of Technology in Zürich (ETHZ), Met Office Hadley Centre (MOHC). See table S1 referencing the RCM deep convection parameterizations.

Name	Institute	GCM	RCM	CPM	Time periods
HCLIMcom	SMHI/FMI/DMI/ Met Norway	EC-EARTH2.2-r12i1p1 (Hazeleger *et al* 2012)	HCLIM38-ALADIN 12 km (Belušić *et al* 2020)	HCLIM38-AROME 3 km (Médus *et al* 2022)	1996–2005 2090–2099
CNRM	Météo France CNRM	CNRM-CM5 (Voldoire *et al* 2013)	CNRM-ALADIN63 12 km (Nabat *et al* 2020)	CNRM-AROME41t1 2.5km (Caillaud *et al* 2021)	1996–2005 2090–2099
KNMI	KNMI	EC-EARTH2.3 (Hazeleger *et al* 2012) member 14 member 4	RACMO2.2 12 km (van Meijgaard*et al* 2008, De Vries *et al* 2022)	HCLIM38-AROME 2.5 km (Belušić *et al* 2020)	 1996–2005 2090–2099
ETHZ	ETHZ	ERA-interim ERA-interim+MPI-ESM-LR r1 Pseudo Global Warming	COSMO-CLM 12 km	COSMO-CLM 2.2 km (Leutwyler *et al* 2017)	1999–2008 2079–2089
MOHC	MOHC	HadGEM3-GC3.1-N512 25 km	None	HadREM3-RA-UM10.1 2.2km (Chan *et al* 2020)	1999–2008 2095–2105

shallow convection within the dry intrusion (Pfahl and Sprenger 2016). We also removed all the data points within the Mediterranean region to focus on Central and Northern Europe (up to 63 N), where models agree on the sign of precipitation change. We used WBPT at 850 hPa (θ_w) to separate storm sectors as it incorporates both temperature and humidity fields. θ_w is preferred over θ as its inclusion of temperature and humidity, which change in the same direction across fronts, allows a better separation of storm sectors (Hewson 1937). It is also a good indicator of frozen precipitation when it is below 273 K (Knox *et al* 2017). θ_w at 850 hPa is directly output by the MOHC and CNRM models. For the other models, we calculated it using temperature and specific or relative humidity (RH). Following Knox *et al* (2017), we developed a simple but accurate formula for the 850 hPa θ_w (supplementary material and figure S1).

2.2.4. Storm intensity

We define the storm intensity as the difference between the SLP minimum at the storm centre and the average SLP on a 2° radius around it to avoid variations in the climatological mean, following Pfahl and Sprenger (2016).

2.2.5. Definition of storm sectors

Figure 2 illustrates a few storm samples. We regrid the CPMs onto the RCM grid via conservative remapping, which means a 12 km grid for most models except MOHC, for which the GCM has a 25 km resolution. Following the simplest way of defining frontal zones provided in Thomas and Schultz (2019), we use the moderate baroclinic zone definition of Sanders (1999) to define fronts as zones where the norm of θ_w gradients is larger than 4 K/110 km on the 25 km MOHC grid. This value is too low for the 12 km RCM grids (too many non-frontal gradients included) so we use 5 K/110 km for them. Sensitivity analysis on the thresholds used to define the fronts do not change the main results as long as the threshold is not too low, which would select small scale frontal structures outside the main ones. We then take the median of θ_w values in this zone to separate a cold sector and a warm sector. As illustrated in figure 2, precipitation in the warm sector is associated with the warm conveyor belt ascent, the cold front and part of the warm front. In this definition of the cold sector, precipitation is mostly coming from shallow convection in the dry intrusion and precipitation ahead of the warm front, in the cloud head. Finally, we also define a central sector (within a 2° radius of the storm centre), where convection is also likely to happen. These definitions are computationally simple and require few variables to provide a first order understanding of which parts of the storms contribute most to precipitation increase.

3. Results

3.1. Winter mean precipitation changes

Figure 1 shows mean precipitation increases by 15%–40% over Northern Europe at the end of the century. MOHC model shows the largest changes, and the CPM amplifies the change by a further 10%–20%. In contrast, the other CPMs have mean changes closer to their parent RCM. Figure S2 shows that this ensemble is representative of the range of precipitation changes in traditional convection-parameterised ensembles over the largest box shown in figure 1.

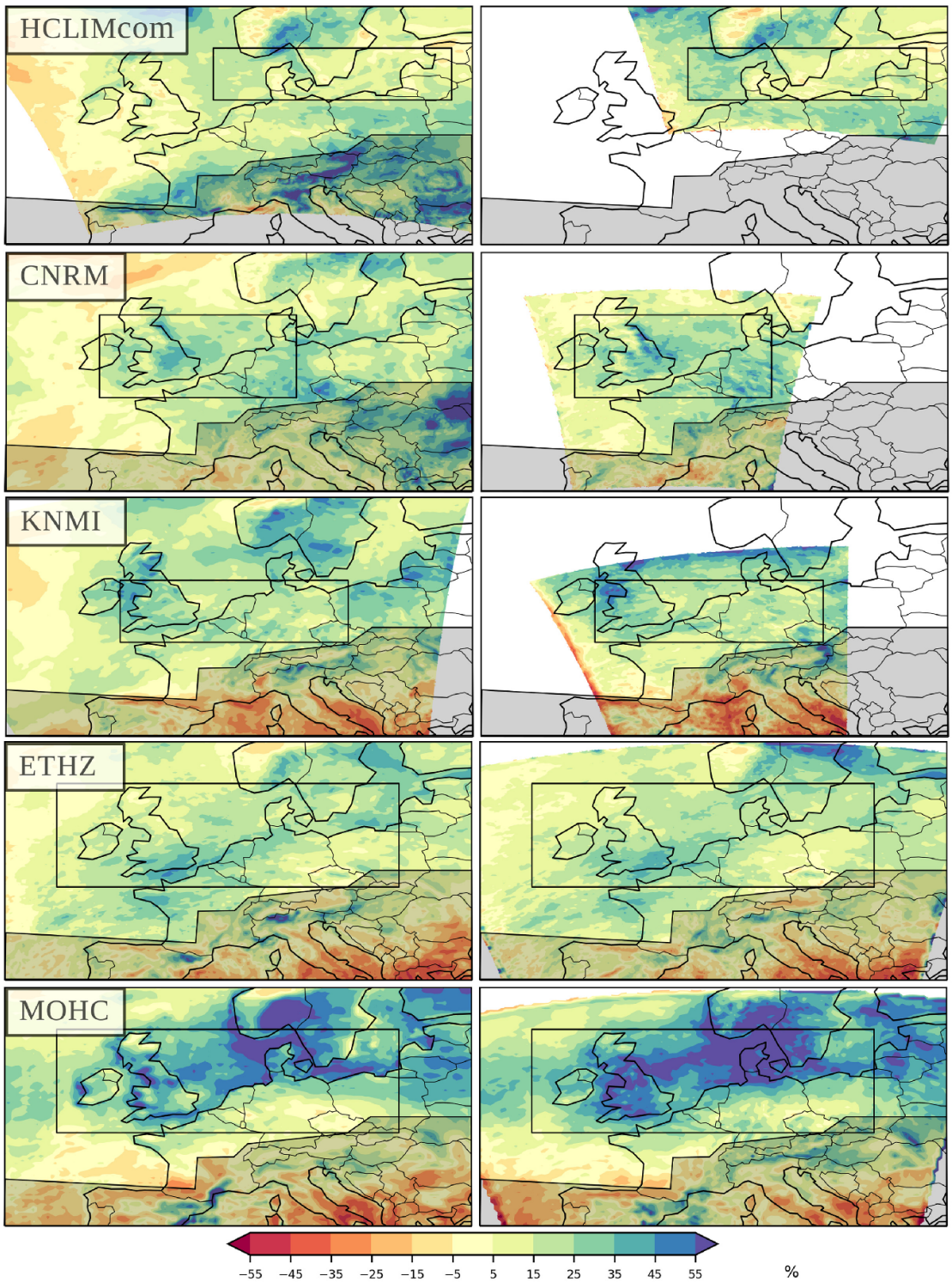

Figure 1. Percentage change in mean winter precipitation at the end of the century compared to the reference period. Left: convection-parameterised models (RCMs), right: convection-permitting models (CPMs). The box shows where storm tracks are selected: (named 'Baltic' for HCLIMcom, 'North Sea' for CNRM and KNMI and 'North Sea & Baltic' for ETHZ and MOHC). The greyed-out Mediterranean zone is removed from the analysis.

Figure S3 further highlights that mean precipitation increase comes from the top half of the precipitation intensity distribution. Models agree on this and there is little land sea contrast in this change. However, the magnitude is different between models, from a 30% increase in the top half of the distribution in most models to a doubling in MOHC models. The further increase in the MOHC CPM also comes from the top half of the distribution. With the same model on a smaller domain, (Kendon *et al* 2020) showed that about half of the larger increase in precipitation was linked with better ability for shower advection over land in the CPM compared to the RCM. We further investigate this from the perspective of precipitation within storms to understand where the remaining differences come from, as well

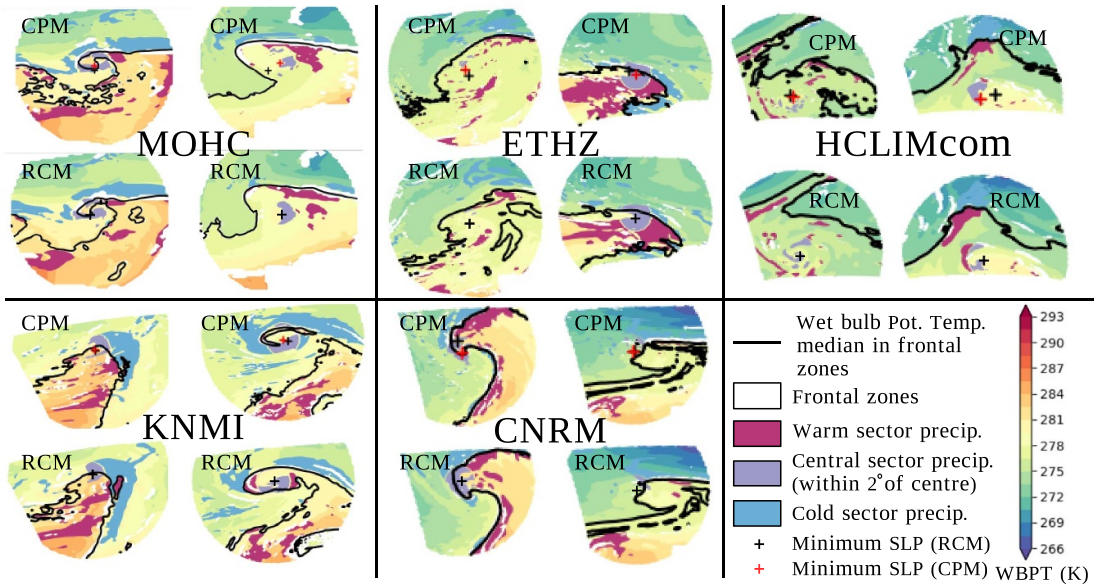

Figure 2. Examples of storms selected for each model: two different storms (left/right) in the CPM (top) or RCM (bottom). Storm sector definitions are explained in the legend, frontal zones are defined as areas with the norm of wet bulb potential temperature (WBPT) gradients stronger than 5 K/110 km (or 4 km/110 km for MOHC model on a 25 km grid).

as whether similar amplification happens in other models. From figure S3, ETHZ CPM is very close to its RCM and CNRM, KNMI and HCLIMcom CPM models have a shifted distribution towards higher intensities, which translates into larger changes in the tail of the distribution.

3.2. Precipitation increases dominated by the warm sector

Interestingly, the increases in the top half of the distribution seen in the precipitation climatology (figure S3) are also found for in-storm precipitation (figure 3). This emphasizes that the dominant mechanism for increased precipitation in winter is more precipitation per storm, consistent with Catto *et al* (2019). For the MOHC models, the larger increases in the CPM (plain line) compared to the RCM (dashed line) shown in the climatology (figure S3) are also found inside storms (figure 3), indicating that the processes generating RCM/CPM differences happen within storms.

By breaking down the precipitation distribution by sectors (defined in section 2.2.5), we show that about two thirds of precipitation comes from the warm sector of storms in present-day winter storms, and most of the intense precipitation happens there. Intense precipitation also happens within the storm centre, but it is a smaller contributor. Frontal zones as defined here are a small contributor, mostly because of their small area.

Looking at future changes, models agree that the warm sector is the main contributor to future changes for the top half of the precipitation distribution. In all models, the increased precipitation contribution from the cold sector peaks at lower precipitation rates (1.5–2 mm h^{-1}) compared to the warm sector. Compared to other models, the MOHC models show a larger contribution to precipitation change from the cold sector, likely linked to increases in the size of the cold sector of storms in these models, as discussed later in section 3.4.

There is also moderate agreement among models that the largest difference between CPMs and RCMs in terms of future changes in precipitation is found for the heaviest precipitation in the warm sector of storms. CNRM, KNMI, MOHC and HCLIMcom CPMs all show significant larger increases in the warm sector for rates above 4 mm h^{-1}. Indeed, at these high rates, the dashed red line representing the RCM is often below the red-shaded range of CPM changes in figure 3. Except in the MOHC model, these larger CPM increases at high rates have a small impact on mean increase.

Larger increases in precipitation in the MOHC CPM compared to the RCM come equally from the cold and warm sectors. The larger increase in cold sector precipitation in the CPM is consistent with the findings of Kendon *et al* (2020), who diagnosed shallow convection and showed it propagates into land in the CPM, and not the RCM. They quantified that this explained 60% of the larger increase in the CPM over land. Figure 3 shows that the rest of the CPM rainfall increase comes from the warm sector. We will explore this in section 3.4.

3.3. Thermodynamical changes dominate the precipitation increase

We now investigate the sources of the spread in projections of mean hourly precipitation per storm between RCMs and the difference in projected

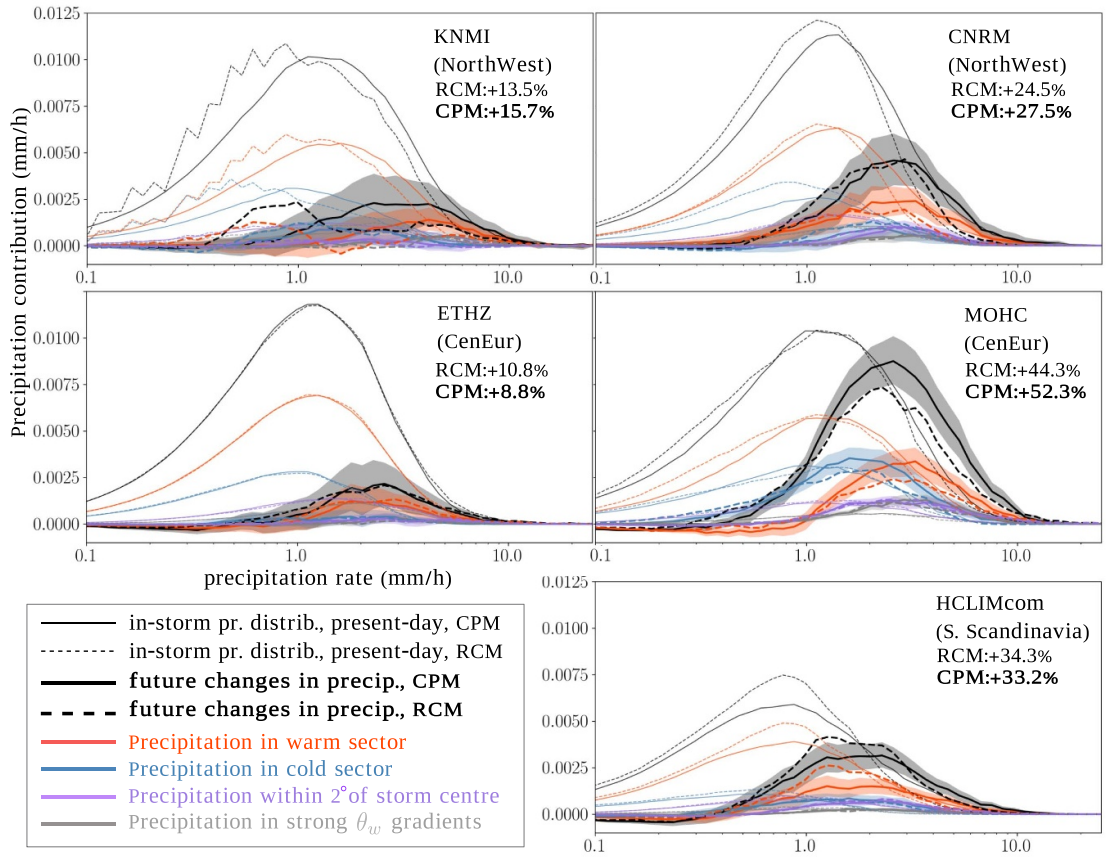

Figure 3. Winter precipitation contribution to the mean within storms (frequency × value of bin, using exponential bins defined in Berthou *et al* 2019). This way, the area under the curve represents mean precipitation (thin lines show present-day contribution) or mean precipitation change (thick lines show future changes, number (%) indicates mean change). Contribution from all points in storms (black), points in warm sector (red), cold sector (blue), central sector (purple) and fronts (grey)—defined in figure 2. Plain line is for CPM, dashed line for RCM. Shading shows the 2.5–97.5 percentile range of CPM precipitation changes using a 1000 bootstrap resampling on storms.

changes for moderate to heavy precipitation in CPMs compared to RCMs. Because the warm sector is a dominant contributor to mean precipitation and precipitation changes, we use median θ_w in the warm sector to scale the spatial mean and 99th percentile of hourly precipitation in storms in figures 4 and S4.

The relationship between median θ_w in the warm sector and hourly mean precipitation is robust, with Pearson correlation coefficient (R) above 0.5 for most models in present-day winter and FW (figure 4). Note that this relationship is less robust if using the whole storm median θ_w, consistent with the warm sector being the largest contributor to in-storm total precipitation and changes (figure 3). These high correlations and the fact that the present-day and future slopes are similar suggest that the first-order driver of increased precipitation per storm is the increase in temperature in the warm sector. The slope ranges between 8% K^{-1} and 14.2% K^{-1} in present-day winters and 9.7%–13.6% K^{-1} in FWs, depending on models and regions. This is above the Clausius–Clapeyron 6%–7% rate (thin black lines in figure 4). This is potentially explained by the fact that storm precipitation also depends on storm dynamical intensity (R between 0.2 and 0.4 (not shown)), in line with Pfahl and Sprenger (2016), and storm intensity is lower at lower θ_w in the warm sector (R between 0.1 and 0.2). To illustrate mean precipitation dependency on dynamical intensity, we added dots to highlight the strongest storms (minimum SLP depression <-5 hPa) in intensification phase (decreasing minimum SLP trend, Catto and Raveh-Rubin (2019)). They are all above the fitted line, confirming that for a given θ_w range, intense storms reach larger precipitation rates.

The models with an increasing proportion of these dynamically strong storms in the future (MOHC, HCLIMcom and CNRM, table 2) tend to have a steeper mean precipitation increase per degree of θ_w in the future (although other factors may play a role in the similar present and future trends in MOHC). In the KNMI model, storms become less dynamically intense (table 2 and figure S5(a)), and the slope is less steep in the future. This illustrates model disagreement in how mean storm dynamical intensity will change (Catto *et al* 2019), and consequently how it will modulate thermodynamical precipitation increase.

Figure 4 also shows the fitted line for present-day autumn (PDA) storms in grey, to explore the hypothesis that the relationship between precipitation and

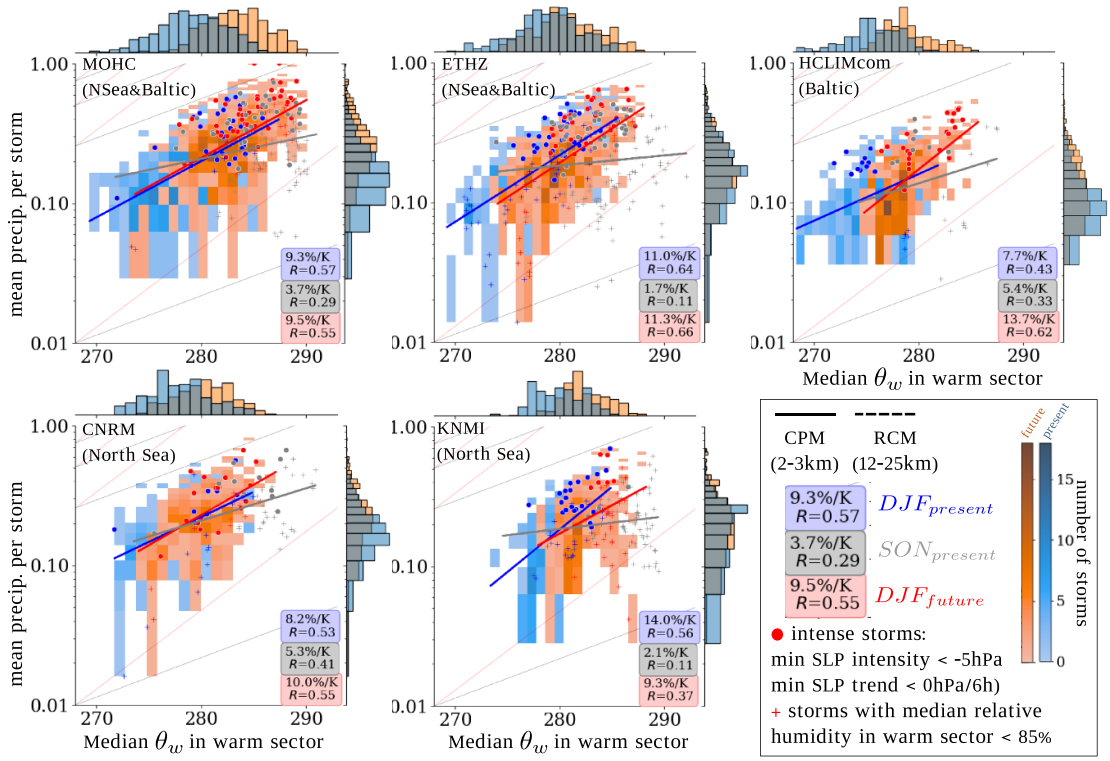

Figure 4. Joint density of mean hourly precipitation per storm and warm sector wet bulb potential temperature (median) in present storms (blue) and future (red). Individual variable density shown at the top (WBPT) and right (mean precipitation). Each panel shows a different model pair. Plain line shows best fit for the CPM, dotted line for the RCM. Grey line is for present-day autumn storms (underlying density not shown). Slope in % K^{-1} and Pearson correlation coefficient are given in insets. Dots represent intense storms; crosses are storms with low relative humidity in their warm sector. Thin grey lines represent Clausius–Clapeyron (CC) 7% K^{-1} scaling and thin red lines show 2×CC scaling.

Table 2. Proportion of intense storms and storms with low median relative humidity in their warm sector.

Model name	Intense storm DJF present	Intense storm DJF future	Intense storm SON present	Low RH DJF present	Low RH DJF future	Low RH SON present
MOHC	4.8%	8.2%	5.1%	0.8%	3%	12.8%
ETHZ	6.3%	6.3%	7.0%	9.4%	3.7%	19.2%
HCLIMcom	2.9%	6.0%	2.7%	1.6%	0%	4.1%
CNRM	2.5%	6.5%	3.6%	5.0%	3.2%	7.7%
KNMI	9.7%	2.7%	8.0%	13.2%	15.5%	20.7%

θ_w in FW storms may be similar to PDA storms. However, the correlation coefficient and slope for PDA storms are much lower for all models. Their intensity is not the main explanation (table 2), although figure S6(a) suggests the median PDA storm is less intense. The largest differences between PDA and FW storms is the median RH in the warm sector which is 2%–6% higher in FW storms than in PDA storms (figure S6(b)). To highlight this, we added crosses for storms with RH below 84% in figure 4. Most of these crosses are below the fitted line in present-day winter and FW: for a given θ_w, storms with lower RH have less precipitation. The proportion of storms with low RH changes from 0% to 15.5% in present winter and FW to 4%–20% in PDA (table 2). PDA storms are therefore limited by lower RH at higher temperature. In contrast, RH in the warm sector of winter storms remains, in future, significantly higher than in PDA storm (figure S6(b)). This explains why FW storms could become as or more rainy than PDA storms while remaining 1 to 2 K cooler (figures S6(c) and (d)).

Figure S4 shows that the 99th percentile of precipitation in PDA storms (ranging from 1 to 9 mm h^{-1}) does reach a similar slope and correlation coefficient as FW storms, suggesting that lower RH in PDA is reducing mean precipitation by reducing lower precipitation rates.

We now investigate the difference in projected changes for moderate to heavy precipitation in CPMs compared to RCMs (for all CPMs apart from ETHZ, figure 3). Figure S4 shows that the slopes between the 99th percentile of precipitation and median θ_w is similar between CPMs and RCMs (when $R > 0.4$), but CPM values are shifted higher. This shift is especially large in PDA storms and FW storms, suggesting that fine-scale processes at larger θ_w values contribute to heavier precipitation in CPMs.

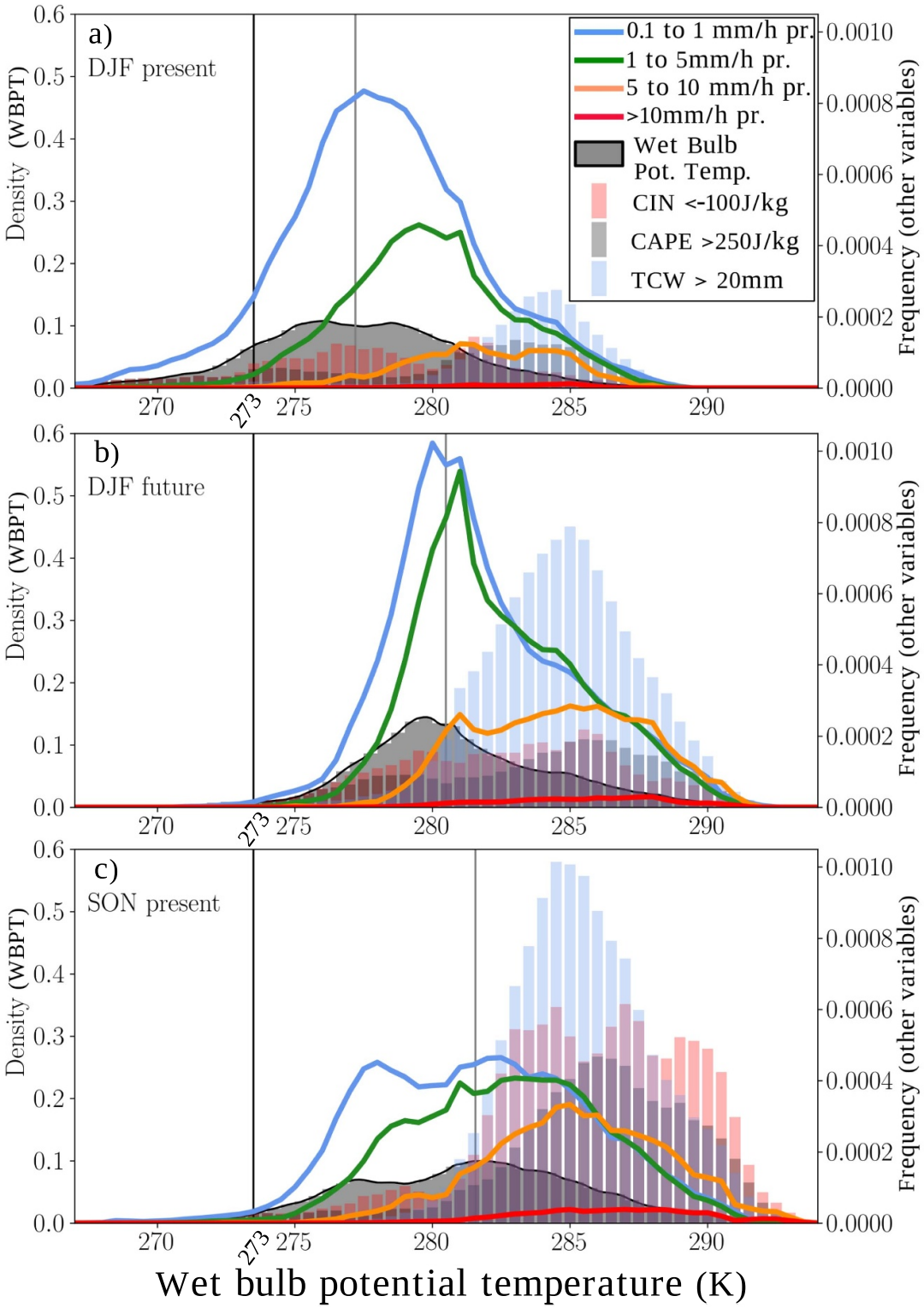

Figure 5. Density of 850 hPa WBPT (black line with grey shading, left axis). Frequency (right axis) of low precipitation rates (0.1–1 mm h^{-1}) scaled by 1/15, moderate rates (1–5 mm h^{-1}) scaled by 1/10, intense rates (5–10 mm h^{-1}) and heavy rates (>10 mm h^{-1}), CAPE (>250 J kg) and CIN (<−100 J kg^{-1}) scaled by 1/10, total column water (TCW >20 mm) scaled by 1/30, binned by θ_w values and normalised by the number of points in all storms on the native grid of the MOHC CPM. Grey vertical line is median θ_w, black vertical line is the freezing point.

The MOHC models shows a peculiar behaviour in two ways: the CPM shows more intense 99th values only in the future and the cold sector contributes significantly to future changes (figure 3). We will investigate these in the next section.

3.4. Understanding MOHC larger increases in storm precipitation

In figure 5, individual grid-points in storms are pooled and binned by θ_w values. Intense precipitation (>5 mm h^{-1}) in storms occurs at θ_w above

280 K and is accompanied by moderate convective available potential energy (CAPE) (>250 J kg^{-1}). In present-day winter storms, these are infrequent, but they become much more frequent in FW storms. When comparing FW storms with PDA storms, the range of θ_w spanned by all storms is the same: 272–292 K. The proportion of grid-points with intense precipitation is similar between FW storms and PDA storms. The frequency of moderate CAPE, convective inhibition (CIN) and high total column water increase in FW storms, favouring more intense convection (Rasmussen *et al* 2017) in the warm sector of storms. Nevertheless, it remains lower than PDA storms. As shown in figure S5(b) and discussed above, RH in the warm sector remains high in FW storms, higher than PDA storms (figure S6b). Because CIN is closely related to low-level RH (Chen *et al* 2020), higher winter RH may explain why CIN values are not as large as PDA storms. Subsequently, CAPE may be released before it can build up to higher values.

In other models, figure S7 shows that θ_w change is less large than in the MOHC model: FW storms in those models are only half-way between present-day winter and autumn ones, and intense precipitation increases in the warm sector are significant but less large than in the MOHC model.

Regarding the larger increase in cold sector precipitation in MOHC models compared to other models, figure 5 shows a skewed θ_w distribution towards lower temperatures compared to the present-day distribution. Figure S5(e) confirms that the cold sector size increases in the future in the MOHC model. A possible explanation is the change in storm types in this model, with more frequent occurrences of Shapiro–Keyser storms (Manning *et al* 2022). The CPM-RCM difference in rain frequency over land due to the lack of shower advection over land in the RCM shown by Kendon *et al* (2020), already known in present-day weather situations, is enhanced in the future because of the cold-sector size increase in the MOHC model. This process, which can be detected in a differential change in wet-hour frequency between land and sea, with further increases in the CPM over land, is only at play in the MOHC model (figure S8).

Finally, we note that the frequency of conditions for frozen precipitation ($\theta_w < 273$ K) decreases by at least two thirds in all models (figures 5 and S7).

4. Conclusions and discussion

We investigated the changes in hourly precipitation in FW storms (extratropical cyclones) in a multi-model regional ensemble at km-scale resolution together with its driving 12–25 km ensemble. The main difference between the two sets of models is that km-scale models allow an explicit representation of convective precipitation (CPMs).

We showed that our small ensemble of five model pairs give a representative sample of end-of-century FW precipitation projections for Northern Europe as provided by more traditional models (CMIP5, CMIP6, CORDEX) in a strong warming scenario (RCP8.5). Changes in storm numbers depend on the global driving model and on inter-decadal variability, and therefore are not investigated here: we examine hourly precipitation within 10° of low-pressure centres.

Our main results are that mean precipitation will increase in FW storms, due to increased moderate and intense precipitation. This increase mostly comes from the warm sector of storms. Differences between models are linked with differences in their warming levels in the warm sector of storms and differences in changes in dynamical strength of storms. The latter is less certain, with little model agreement (Catto *et al* 2019), also potentially because dynamical strength is more prone to inter-decadal variability. Our small ensemble design is too limited to address this.

Because WBPT ranges in FW storms may reach similar values to PDA ones, we compare both sets of storms. Hourly mean precipitation in FW storms reaches larger values than PDA storms because FW storms have higher RH in their warm sector, and more light precipitation. Intense (>5 mm h^{-1}) and heavy (>10 mm h^{-1}) precipitation within winter storms increase in frequency, and get closer to (or even up to for one model) PDA storms. The frequency of favourable conditions for frozen precipitation also gets closer to PDA storms, with a decrease by at least two thirds in frequency.

The warm sector increase in precipitation is likely linked with more convection, as shown by CAPE and CIN increases in the MOHC model, which is coherent with other CPMs also showing a greater increase in intense precipitation rates (>4 mm h^{-1}) than RCMs in this sector. A particular feature of the MOHC CPM is a larger increase in precipitation in the cold sector, likely linked with a deficiency in the RCM to advect showers over land (Kendon *et al* 2020). This may be because this model shows the largest increase in cold sector size in future storms or it may be a particular feature of the convection scheme used in the MOHC RCM.

This study shows that the magnitude of the larger increase in mean precipitation in the MOHC CPM is not found in other RCM/CPM pairs. We therefore recommend consideration of multi-model ensembles when possible. We showed that CPMs are useful tools to better understand changes in intense rain rates and fine-scale processes in winter storms. Nevertheless, levels of warming within the warm sector of storms and dynamical strength of storms, well captured by RCMS, are the largest factors explaining mean hourly precipitation changes in storms.

Data availability statement

The data that support the findings of this study are openly available at the following URL/DOI: https://doi.org/10.5281/zenodo.6883357.

Acknowledgments

This study received support from the European Union's Horizon 2020 EUCP project (Grant No. GA776613). NB UIBK and ETHZ acknowledge PRACE for awarding us the access to Piz Daint at Swiss National Supercomputing Center (CSCS, Switzerland) and the COSMO, CLM and C2SM communities for developing and maintaining COSMO in climate mode. CM is supported by the UKRI NERC funded project STORMY-WEATHER (Grant No. NE/V004166/1). DB was partially funded by the Formas project EDUCAS (Grant No. 2019-00829). S B, M J R and E K gratefully acknowledge support from the Joint UK BEIS/Defra Met Office Hadley Centre Climate Programme (Grant No. GA01101).

ORCID iDs

Ségolène Berthou https://orcid.org/0000-0002-9164-0841
Malcolm J Roberts https://orcid.org/0000-0001-6128-6979
Benoît Vannière https://orcid.org/0000-0001-8600-400X
Nikolina Ban https://orcid.org/0000-0002-1672-3655
Danijel Belušić https://orcid.org/0000-0002-5665-3866
Cécile Caillaud https://orcid.org/0000-0003-2317-4129
Thomas Crocker https://orcid.org/0000-0001-7761-5546
Hylke de Vries https://orcid.org/0000-0002-6124-1102
Dan Harris https://orcid.org/0000-0003-4369-4674
Elizabeth J Kendon https://orcid.org/0000-0003-1538-2147
Oskar Landgren https://orcid.org/0000-0002-6264-8502
Colin Manning https://orcid.org/0000-0001-5364-3569

References

Albern N, Voigt A and Pinto J G 2021 Tropical cloud-radiative changes contribute to robust climate change-induced jet exit strengthening over Europe during boreal winter *Environ. Res. Lett.* **16** 084041

Ban N *et al* 2021 The first multi-model ensemble of regional climate simulations at kilometer-scale resolution, part I: evaluation of precipitation *Clim. Dyn.* **57** 275–302

Belušić D *et al* 2020 HCLIM38: a flexible regional climate model applicable for different climate zones from coarse to convection-permitting scales *Geosci. Model Dev.* **13** 1311–33

Berthou S, Kendon E J, Chan S C, Ban N, Leutwyler D, Schär C and Fosser G 2020 Pan-European climate at convection-permitting scale: a model intercomparison study *Clim. Dyn.* **55** 35–59

Berthou S, Kendon E J, Rowell D P, Roberts M J, Tucker S and Stratton R A 2019 Larger future intensification of rainfall in the West African Sahel in a convection permitting model *Geophys. Res. Lett.* **46** 13299–307

Brogli R, Sørland S L, Kröner N and Schär C 2019 Causes of future Mediterranean precipitation decline depend on the season *Environ. Res. Lett.* **14** 114017

Browning K A 1997 The dry intrusion perspective of extra-tropical cyclone development *Meteorol. Appl.* **4** 317–24

Caillaud C, Somot S, Alias A, Bernard-Bouissières I, Fumière Q, Laurantin O, Seity Y and Ducrocq V 2021 Modelling Mediterranean heavy precipitation events at climate scale: an object-oriented evaluation of the CNRM-AROME convection-permitting regional climate model *Clim. Dyn.* **56** 1717–52

Catto J L, Ackerley D, Booth J F, Champion A J, Colle B A, Pfahl S, Pinto J G, Quinting J F and Seiler C 2019 The future of midlatitude cyclones *Curr. Clim. Change Rep.* **5** 407–20

Catto J L and Raveh-Rubin S 2019 Climatology and dynamics of the link between dry intrusions and cold fronts during winter. Part I: global climatology *Clim. Dyn.* **53** 1873–92

Chan S C, Kendon E J, Berthou S, Fosser G, Lewis E and Fowler H J 2020 Europe-wide precipitation projections at convection permitting scale with the Unified Model *Clim. Dyn.* **55** 409–28

Chen J, Dai A, Zhang Y and Rasmussen K L 2020 Changes in convective available potential energy and convective inhibition under global warming *J. Clim.* **33** 2025–50

Chen T-C, Yau M-K and Kirshbaum D J 2021 Sensitivities of slantwise convection dynamics to model grid spacing under an idealized framework *Q. J. R. Meteorol. Soc.* **147** 1930–48

De Vries H, Lenderink G, van der Wiel K and van Meijgaard E 2022 Quantifying the role of the large-scale circulation on European summer precipitation change *Clim. Dyn.* **59** 2871–86

Doblas-Reyes F J *et al* 2021 Linking global to regional climate change *Climate Change 2021: The Physical Science Basis. Contribution of Working Group I to the Sixth Assessment Report of the Intergovernmental Panel on Climate Change*, ed D V Masson (Cambridge, UK: Cambridge University Press) ch 10

Fereday D, Chadwick R, Knight J and Scaife A A 2018 Atmospheric dynamics is the largest source of uncertainty in future winter European rainfall *J. Clim.* **31** 963–77

Fischer E M and Knutti R 2016 Observed heavy precipitation increase confirms theory and early models *Nat. Clim. Change* **6** 986–91

Glinton M R, Gray S L, Chagnon J M and Morcrette C J 2017 Modulation of precipitation by conditional symmetric instability release *Atmos. Res.* **185** 186–201

Grossman R L and Betts A K 1990 Air-sea interaction during an extreme cold air outbreak from the Eastern Coast of the United States *Mon. Weather Rev.* **118** 324–42

Harvey B J, Cook P, Shaffrey L C and Schiemann R 2020 The response of the Northern Hemisphere storm tracks and jet streams to climate change in the CMIP3, CMIP5 and CMIP6 climate models *J. Geophys. Res.* **125** e2020JD032701

Hawcroft M, Walsh E, Hodges K and Zappa G 2018 Significantly increased extreme precipitation expected in Europe and North America from extratropical cyclones *Environ. Res. Lett.* **13** 124006

Hazeleger W *et al* 2012 EC-Earth V2.2: description and validation of a new seamless earth system prediction model *Clim. Dyn.* **39** 2611–29

Hentgen L, Ban N, Kröner N, Leutwyler D and Schär C 2019 Clouds in convection-resolving climate simulations over Europe *J. Geophys. Res.* **124** 3849–70

Hewson E W 1937 The application of wet-bulb potential temperature to air mass analysis. III rainfall in depressions *Q. J. R. Meteorol. Soc.* **63** 323–8

Kendon E J, Roberts N M, Fosser G, Martin G M, Lock A P, Murphy J M, Senior C A and Tucker S O 2020 Greater future U.K. winter precipitation increase in new convection-permitting scenarios *J. Clim.* **33** 7303–18

Knox J A, Nevius D S and Knox P N 2017 Two simple and accurate approximations for wet-bulb temperature in moist conditions, with forecasting applications *Bull. Am. Meteorol. Soc.* **98** 1897–906

Lean H W and Clark P A 2003 The effects of changing resolution on mesoscale modelling of line convection and slantwise circulations in FASTEX IOP16 *Q. J. R. Meteorol. Soc.* **129** 2255–78

Leutwyler D, Lüthi D, Ban N, Fuhrer O and Schär C 2017 Evaluation of the convection-resolving climate modeling approach on continental scales *J. Geophys. Res.* **122** 5237–58

Manning C, Kendon E J, Fowler H J, Roberts N M, Berthou S, Suri D and Roberts M J 2021 Extreme windstorms and sting jets in convection-permitting climate simulations over Europe *Clim. Dyn.* **58** 2387–404

Médus E *et al* 2022 Characteristics of precipitation extremes over the Nordic region: added value of convection-permitting modeling *Nat. Hazards Earth Syst. Sci. Discuss.* **22** 693–711

Muchan K, Lewis M, Hannaford J and Parry S 2015 The winter storms of 2013/2014 in the UK: hydrological responses and impacts *Weather* **70** 55–61

Nabat P, Somot S, Cassou C, Mallet M, Michou M, Bouniol D, Decharme B, Drugé T, Roehrig R and Saint-Martin D 2020 Modulation of radiative aerosols effects by atmospheric circulation over the Euro-Mediterranean region *Atmos. Chem. Phys.* **20** 8315–49

Neiman P J, Shapiro M A and Fedor L S 1993 The life cycle of an extratropical marine cyclone. Part II: mesoscale structure and diagnostics *Mon. Weather Rev.* **121** 2177–99

Neu U *et al* 2013 IMILAST: a community effort to intercompare extratropical cyclone detection and tracking algorithms *Bull. Am. Meteorol. Soc.* **94** 529–47

Oertel A, Boettcher M, Joos H, Sprenger M, Konow H, Hagen M and Wernli H 2019 Convective activity in an extratropical cyclone and its warm conveyor belt—a case-study combining observations and a convection-permitting model simulation *Q. J. R. Meteorol. Soc.* **145** 1406–26

Oertel A, Boettcher M, Joos H, Sprenger M and Wernli H 2020 Potential vorticity structure of embedded convection in a warm conveyor belt and its relevance for large-scale dynamics *Weather Clim. Dyn.* **1** 127–53

Pfahl S and Sprenger M 2016 On the relationship between extratropical cyclone precipitation and intensity *Geophys. Res. Lett.* **43** 1752–8

Pichelli E *et al* 2021 The first multi-model ensemble of regional climate simulations at kilometer-scale resolution part 2: historical and future simulations of precipitation *Clim. Dyn.* **56** 3581–602

Poujol B, Mooney P A and Sobolowski S P 2021 Physical processes driving intensification of future precipitation in the mid- to high latitudes *Environ. Res. Lett.* **16** 34051

Priestley M D K and Catto J L 2021 Future changes in the extratropical storm tracks and cyclone intensity, wind speed and structure *Weather Clim. Dyn. Discuss.* **2021** 1–40

Rasmussen K L, Prein A F, Rasmussen R M, Ikeda K and Liu C 2017 Changes in the convective population and thermodynamic environments in convection-permitting regional climate simulations over the United States *Clim. Dyn.* **55** 383–408

Rasp S, Selz T and Craig G C 2016 Convective and slantwise trajectory ascent in convection-permitting simulations of midlatitude cyclones *Mon. Weather Rev.* **144** 3961–76

Sanders F 1999 A proposed method of surface map analysis *Mon. Weather Rev.* **127** 945–55

Thomas C M and Schultz D M 2019 What are the best thermodynamic quantity and function to define a front in gridded model output? *Bull. Am. Meteorol. Soc.* **100** 873–95

Ullrich P A, Zarzycki C M, McClenny E E, Pinheiro M C, Stansfield A M and Reed K A 2021 TempestExtremes v2.1: a community framework for feature detection, tracking and analysis in large datasets *Geosci. Model Dev.* **14** 5023–48

van Meijgaard E, Ulft L H V, Bosveld F C, Lenderink G and Siebesma A P 2008 The KNMI regional atmospheric climate model RACMO version 2.1 *Technical Report TR-302* p 43

Voldoire A *et al* 2013 The CNRM-CM5.1 global climate model: description and basic evaluation *Clim. Dyn.* **40** 2091–121

Zappa G, Shaffrey L C, Hodges K I, Sansom P and Stephenson D 2013 The response of North Atlantic cyclones to climate change in CMIP5 models *J. Clim.* **26** 5846–62

Zarzycki C M and Ullrich P A 2017 Assessing sensitivities in algorithmic detection of tropical cyclones in climate data *Geophys. Res. Lett.* **44** 1141–9